

# Water-Soluble, Electroactive, and Photoluminescent Quaterthiophene–Dinucleotide Conjugates

Silvia Alesi, Giorgia Brancolini, Manuela Melucci, Massimo Luigi Capobianco, Alessandro Venturini, Nadia Camaioni, and Giovanna Barbarella\*<sup>[a]</sup>

**Abstract:** Quaterthiophene–dinucleotide conjugates  $5'$ TA $3'$ –t4 $3'$ AT $5'$ ,  $5'$ AA $3'$ –t4 $3'$ AA $5'$ , and  $5'$ TT $3'$ –t4 $3'$ TT $5'$  (TA: thymidine–adenosine, AA: adenosine–adenosine, TT: thymidine–thymidine) were synthesized and analyzed by a combination of spectroscopy and microscopy, electrical characterization, and theoretical calculations. Circular dichroism (CD) experiments demonstrated a transfer of chirality from the

dinucleotides to quaterthiophene at high ionic strength and in cast films. The films were photoluminescent and electroactive. CD and photoluminescence spectra and current density/voltage plots (measured under dynamic

vacuum) displayed significant variation on changing the dinucleotide scaffold. Molecular mechanics and molecular dynamics calculations indicated that the conformation and packing modes of the conjugates are the result of a balance between intra- and intermolecular nucleobase–thiophene stacking interactions and intramolecular hydrogen bonding between the nucleobases.

**Keywords:** charge mobility • circular dichroism • oligonucleotides • photoluminescence • thiophene

## Introduction

Thiophene oligomers and polymers are among the most investigated semiconductor materials for organic electronics.<sup>[1]</sup> Generally, to make them soluble in organic solvents, alkyl chains, aryl groups, and a variety of other substituents are grafted onto the aromatic backbone. A few polythiophenes with charged-pendant groups, which make them soluble in water, have also been described and used as optical transducers in biosensors for the detection of DNA mismatches in pathological samples.<sup>[2]</sup> Water-soluble conjugated polyelectrolytes offer many opportunities to reveal chemical and biochemical events through changes in absorption or photoluminescence signals, electrical conductivity, or redox potentials.<sup>[2–3]</sup> The methodologies that employ cationic polythiophene transducers to detect biomolecules have been demonstrated to be very sensitive and specific.<sup>[2]</sup> As a result of the

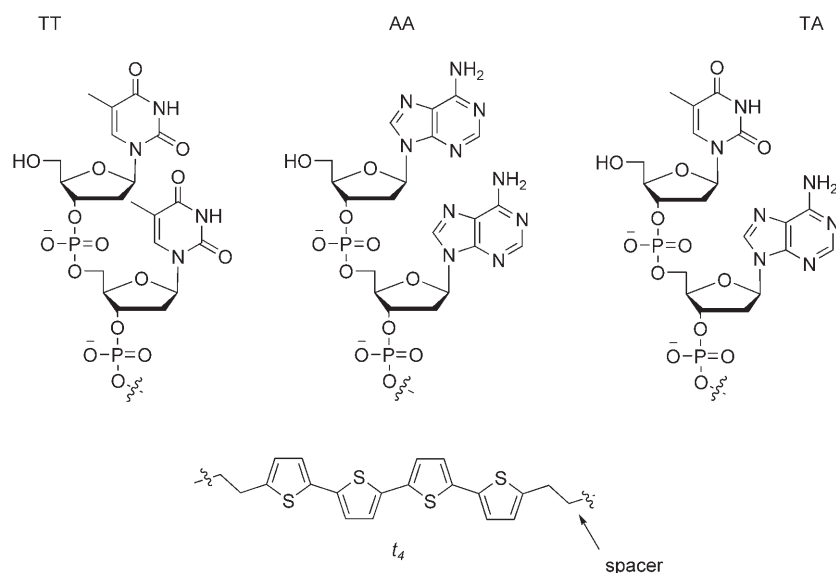
ready read-out modalities and high sensitivity, fluorescence detection is the most employed technique for biosensors based on cationic polythiophenes.<sup>[2–3b]</sup>

On these grounds, we focused our attention on the use of oligonucleotides—readily available and easy to graft onto organic molecules by means of known methodologies—as scaffolds to prepare water-soluble functional molecules capable, on one hand, to recognize the presence of relevant biomolecules in physiological/pathological processes and, on the other, to self-assemble over different length scales in thin films through biomolecular recognition. We aimed, in particular, at developing theoretical and experimental tools to understand the interactions of thiophene derivatives with DNA components by means of the synthesis of oligothiophene–oligonucleotide hybrid structures and to study the way they interact and organize in solution and thin film. “Biohybrid” materials made of organic and bio-organic segments are an emerging research area in the field of materials science.<sup>[4]</sup> However, so far, very few compounds combining thiophene-based segments with DNA components (mainly nucleosides) have been reported.<sup>[5]</sup>

We report herein an investigation concerning the synthesis and characterization of a structurally homogeneous set of quaterthiophene–dinucleotide conjugates, in which the thiophene oligomer is linked to thymidine–adenosine (TA), adenosine–adenosine (AA), and thymidine–thymidine (TT) dinucleotides at both terminal positions (Scheme 1).

[a] Dr. S. Alesi, Dr. G. Brancolini, Dr. M. Melucci, Dr. M. L. Capobianco, Dr. A. Venturini, Dr. N. Camaioni, Dr. G. Barbarella  
Consiglio Nazionale Ricerche  
CNR-ISOF, Via P. Gobetti 101  
40129 Bologna (Italy)  
Fax: (+39)051-639-8349  
E-mail: barbarella@isof.cnr.it

Supporting information for this article is available on the WWW under <http://www.chemeurj.org/> or from the author.



Scheme 1. The molecular structure of the building blocks of conjugates  ${}^5\text{TA}^3\text{-t4-}^3\text{AT}^5$ ,  ${}^5\text{AA}^3\text{-t4-}^3\text{AA}^5$ , and  ${}^5\text{TT}^3\text{-t4-}^3\text{TT}^5$ .

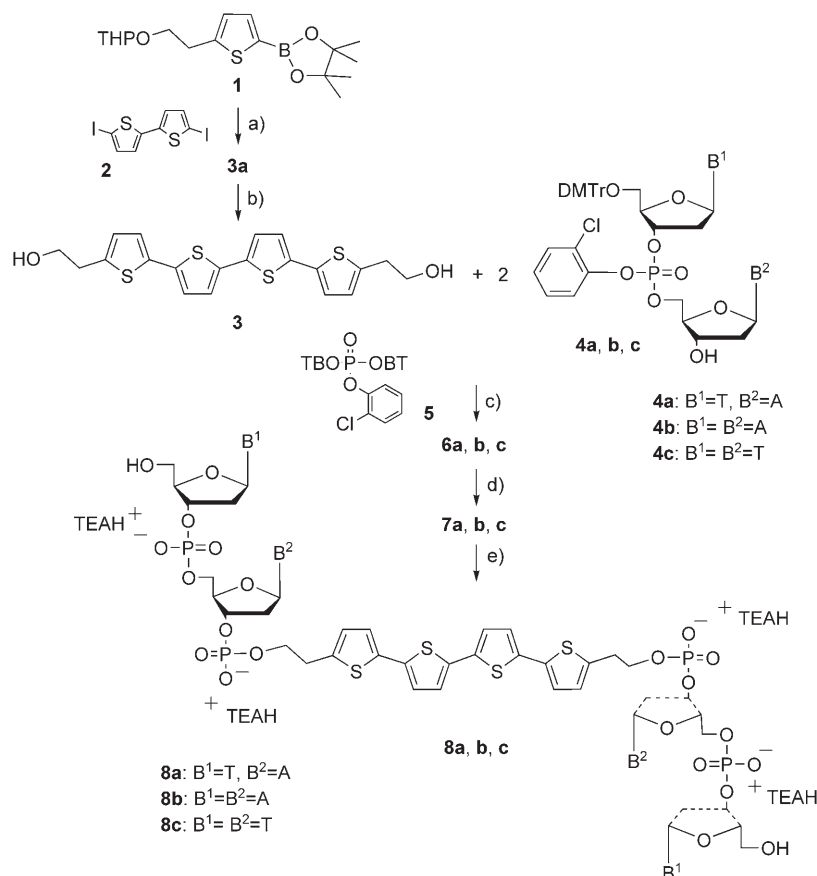
Quaterthiophene is one of the most investigated thiophene derivatives for its semiconductor<sup>[6a]</sup> and photoluminescent properties.<sup>[6b]</sup> TA, AA, and TT dinucleotides were linked to the quaterthiophene backbone through an ethylene spacer to confer conformational flexibility to the structure.

By means of a combination of spectroscopic methods, fluorescence microscopy, electrical characterization, and theoretical calculations, we demonstrate that the bioconjugates are photoluminescent and electroactive compounds and that their conformational preferences and packing modalities originate from a critical balance between intra- and intermolecular nucleobase–thiophene stacking interactions and intramolecular hydrogen bonds formed by the nucleobases.

## Results and Discussion

**Synthesis:** Conjugates  ${}^5\text{TA}^3\text{-t4-}^3\text{AT}^5$ ,  ${}^5\text{AA}^3\text{-t4-}^3\text{AA}^5$ , and  ${}^5\text{TT}^3\text{-t4-}^3\text{TT}^5$  were prepared following the synthetic pattern shown in Scheme 2, thus taking advantage of microwave

assistance in steps (a) and (b) for the preparation of the parent quaterthiophene.<sup>[7]</sup> Quaterthiophene **3** with protected alcoholic groups was obtained in 87% yield in 5 min through the solvent-free, microwave-assisted coupling of diiodo derivative **2** with boronic ester **1** using  $[\text{PdCl}_2(\text{dppf})]/\text{KF}$  and  $\text{Al}_2\text{O}_3/\text{KOH}$  (10% aq.) as a catalytic system. After deprotection under microwave activation, the oligomer was treated with an excess of 5'-protected (4,4'-dimethoxytrityl)deoxy dinucleotides **4a–c** previously phosphorylated with 2-chlorophenyl-*O,O*-bis-(1-benzotriazolyl)phosphate in pyridine as the solvent. After removal of the 5'-dimethoxytrityl group with benzenesulfonic acid, the detritylated compound was treated with  $N^1,N^1,N^3,N^3$ -tetramethylguanidine and *syn*-pyri-



Scheme 2. a)  $\text{KF}$ ,  $[\text{PdCl}_2(\text{dppf})]$ ,  $\text{Al}_2\text{O}_3/\text{KOH}$  (10% aq.), MW, 5 min; b)  $\text{HCl}$  (0.2N), THF, MW, 5 min; c) **5**, py, 2 h, RT; d) benzenesulfonic acid,  $\text{MeOH}/\text{CH}_2\text{Cl}_2$ , 0.5 h, RT; e) py, 16 h, RT;  $\text{NH}_3$  (30% aq.), 24 h, 50°C. BT = benzotriazolyl, DMTr = 4,4'-dimethoxytrityl, dppf = 1,1'-bis(diphenylphosphino)ferrocene, MW = microwave, py = pyridine, THP = tetrahydropyran, TEA = triethylamine.

dine-2-carboaldoxime and then with aqueous ammonia. The target compounds **8a–c** were obtained from the crude mixture after reversed-phase chromatography and characterized by mass spectrometry,  $^1\text{H}$  and  $^{31}\text{P}$  NMR spectroscopy, UV/Vis spectroscopy, and photoluminescence (PL) (further synthetic and characterization details are given in the Supporting Information).

**Optical properties (UV, PL, and CD):** Conjugates **8a–c** are photoluminescent compounds in solution in water and in cast films. The UV/Vis and PL spectra in water and in films cast from  $10^{-3}\text{M}$  solutions in water are shown in Figure 1a

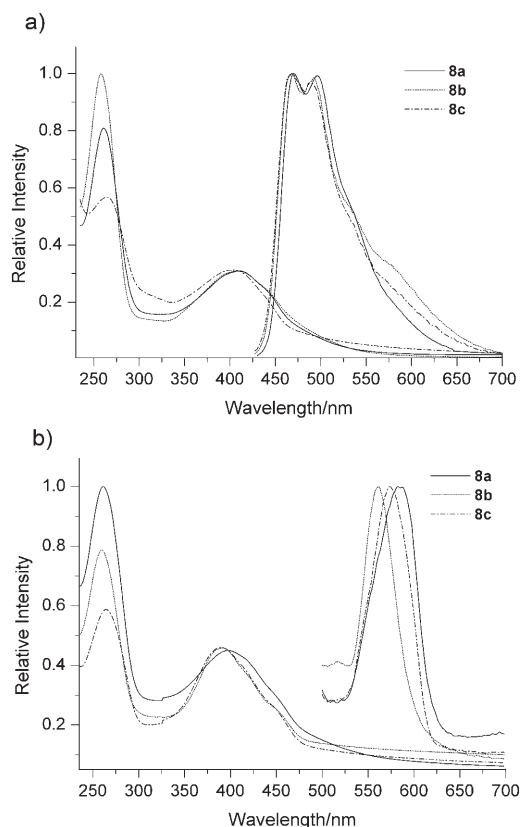


Figure 1. UV/Vis and PL spectra ( $\lambda_{\text{exc}}=410\text{ nm}$ ) of conjugates  $^5\text{TA}^3\text{-t4-}^3\text{AT}^5$ ,  $^5\text{AA}^3\text{-t4-}^3\text{AA}^5$ , and  $^5\text{TT}^3\text{-t4-}^3\text{TT}^5$  (**8a–c**) in a) water and b) films cast from a  $10^{-3}\text{M}$  water solution.

and 1b, respectively, while the absorption and PL wavelengths are reported in the Supporting Information. The UV/Vis spectra in solution consist of signals around 260 nm, from the oligonucleotide moiety, and 400 nm, from the quaterthiophene t4. The PL spectra in solution, which arise from the t4 moieties, consist of a main signal split into two bands near 500 nm and two red-shifted shoulders in the region 550–600 nm. These spectra are very similar to those of “free” quaterthiophene and, in general, to those spectra of thiophene oligomers in solution.<sup>[7]</sup> The UV/Vis signals of the conjugates in cast films are almost superimposable and are blue-shifted by 10–17 nm with respect to those in solution, whereas the signals pertaining to the dinucleotide scaffold

remain unchanged. Instead, the PL signals of **8a–c** in cast films are remarkably sharpened with respect to the solution, well separated from each other, and red-shifted by 70 to nearly 100 nm. This behavior recalls that shown in the formation of H-type aggregates, such as those described, for example, for *trans*-stilbene in Langmuir–Blodgett films<sup>[8a]</sup> or for supramolecular assemblies of chiral oligothiophenes<sup>[8b]</sup> and indicates that the t4 components form orientationally ordered domains in the film.<sup>[8c]</sup> However, further studies are required to fully elucidate the relationship between the aggregation modalities of **8a–c** and their photophysical properties. Investigations in this direction are currently under way.

Circular dichroism (CD) experiments demonstrated a transfer of chirality from the dinucleotide substituents to the quaterthiophene moiety at high ionic strength and in films. The CD spectra of the bioconjugates in  $10^{-5}\text{M}$  solution in aqueous buffer (pH 7.4), aqueous buffer containing 1 M NaCl, and in cast films from solutions in water are shown in Figure 2. The detailed CD data of **8a–c** are reported in the Supporting Information.

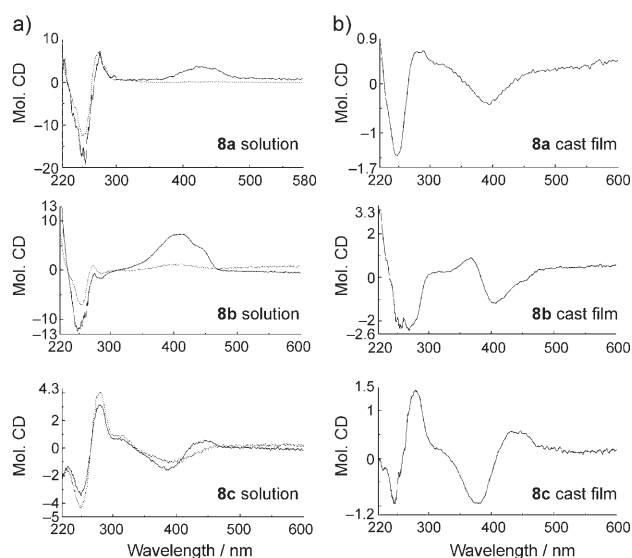


Figure 2. CD spectra of a) conjugates  $^5\text{TA}^3\text{-t4-}^3\text{AT}^5$ ,  $^5\text{AA}^3\text{-t4-}^3\text{AA}^5$ , and  $^5\text{TT}^3\text{-t4-}^3\text{TT}^5$  (**8a–c**) in aqueous buffer (pH 7.4; dotted line) and aqueous buffer with 1 M NaCl (solid line) and b) cast film from  $10^{-3}\text{M}$  solutions in water.

The spectra consist of two regions: one with a bisignated signal at 250–280 nm assigned to the TA, AA, and TT dinucleotides and the other with a signal around 400 nm that corresponds to the  $\pi\text{-}\pi^*$  absorption region of t4 and is related to long-range electronic interactions between the t4 moieties. Upon increasing the ionic strength of the solutions of **8a–c** by the addition of NaCl, which increases molecular aggregation, the dinucleotide signals display only minor variations, while the t4 signals show changes both in intensity and shape. Conjugate **8a** shows a very weak positive signal at 437 nm in aqueous buffer, but the chirality factor  $g$  increases in intensity by more than two orders of magnitude following

the addition of NaCl (see the Supporting Information). Conjugate **8b** shows a weak positive signal at 410 nm with the  $g$  value increasing sixfold upon addition of NaCl. In this case, the increase in the  $g$  value of the signal at 410 nm is accompanied by the appearance of a further weak positive signal near 450 nm. Conjugate **8c** shows a negative and broad signal around 387 nm in aqueous buffer, which upon addition of NaCl gives rise to a nonsymmetric bisignated signal with a stronger negative component at 384 nm and a weaker positive component at 443 nm with zero crossing at 420 nm. The bisignated signal is characteristic of an exciton coupling between chromophores in a chiral orientation.<sup>[9]</sup> In this specific case, it indicates a right-handed helical arrangement of interacting t4 moieties. In cast film, **8c** shows the same bisignated signal displayed in solution at high ionic strength with the zero crossing wavelength blue-shifted to 407 nm. Conjugate **8a** in cast film shows an inverted, negative signal blue-shifted to 400 nm. The behavior of conjugate **8b** in cast film is more complex. The bisignated signal that pertains to the oligonucleotide scaffold becomes broad and there is the appearance of an exciton couplet in the region of t4, which is composed of a negative band at 367 nm and a positive band at 407 nm (zero crossing at 383 nm). This behavior indicates that the interacting t4 moieties are organized in a helical left-handed fashion.<sup>[9]</sup> The spectrum also shows some signals in the region around 450 nm, thus overlapping with the negative part of the bisignated signal.

CD spectroscopy is one of the most sensitive techniques available for the analysis of aggregation modalities in  $\pi$ - $\pi$  conjugated systems.<sup>[9,10]</sup> In the present case, CD spectra indicate fine variations in aggregation modalities of the conjugates on changing the oligonucleotide scaffold. In cast film, the interplay between molecule-molecule and molecule-substrate interactions governs the aggregation process. When molecule-molecule interactions are weak, the interaction of the molecules with the surface drives the formation of the supramolecular aggregate. Sign inversions in the CD spectra from solution to film are also commonly observed in the case of the oligothiophenes.<sup>[8b,d]</sup> The fact that the shape of the spectrum does not change for **8c** from solution to cast film is an indication that the aggregate formed by this conjugate is intrinsically more stable than those formed by **8a** and **8b**.

**Shape of the aggregates:** Conjugates **8a-c** are amphiphilic molecules with hydrophobic (i.e., t4) and hydrophilic (i.e., TA, AA, and TT) moieties. As is typical of amphiphilic compounds,<sup>[11]</sup> the casting of **8a-c** from water leads to the formation of spherical, globular, or even dendritic aggregates depending on the experimental conditions. However, under carefully controlled deposition conditions, we observed the formation of rod-like aggregates for all the conjugates, thus showing that despite the very different intimate nature of the **8a-c** aggregates on surfaces as revealed by CD spectroscopy, their morphological habit in cast film was always the same. This morphology consisted of an amorphous matrix containing numerous randomly oriented rods,

the length of which could reach up to a 100  $\mu$  depending on the rate of solvent evaporation and the hydrophilicity of the surface employed (glass, glass covered with amylose, SiO<sub>2</sub>, and mica were tested). The samples were prepared in a solvent-saturated environment at room temperature to obtain the deposition under quasi-equilibrium conditions: a 50  $\mu$ L aliquot of a 1 mg/200  $\mu$ L solution in water was cast on glass and after complete solvent evaporation ( $\approx$ 12 h) was analyzed under ambient conditions by optical, fluorescence, and atomic force microscopy (AFM; see the AFM image reported in the Supporting Information). No rod-like aggregates were observed when the solvent was quickly removed under vacuum. The longest rods were obtained by employing a surface made of amylose deposited on glass. Upon UV irradiation all the films displayed intense yellow-orange fluorescence emission. Figure 3 shows the fluorescence microscopy image



Figure 3. Fluorescence microscopy image of rod-like aggregates formed by the deposition of <sup>5</sup>AA<sup>3</sup>-t4-<sup>3</sup>AA<sup>5</sup> (**8b**) on a glass substrate covered with a thick layer of amylose.

image of a cast film of <sup>5</sup>AA<sup>3</sup>-t4-<sup>3</sup>AA<sup>5</sup> (**8b**; 40  $\mu$ L, 1 mg mL<sup>-1</sup> solution in H<sub>2</sub>O; the corresponding optical microscopy image is given in the Supporting Information) deposited at room temperature on a glass substrate covered with an amylose layer (50  $\mu$ L, 2 mg mL<sup>-1</sup> solution in dimethyl sulfoxide (DMSO)), therefore showing the formation of rod-like aggregates up to 100  $\mu$  in length. Amylose, a linear polymer of  $\alpha$ -1,4-linked glucose,<sup>[12]</sup> has a helical structure and once cast on glass forms a chiral surface. Thus, it cannot be excluded that chiral-chiral interactions between the chiral surface and the chiral conjugates contribute to the formation of the longest rods. However, since the formation of rod-like aggregates, such as those shown in Figure 3, has never been observed with oligothiophenes, including those made amphiphilic by the presence of ethylene oxide chains,<sup>[8b]</sup> it is reasonable to ascribe their formation to the orienting effect of the dinucleotide scaffolds in **8a-c**.

**Electrical characterization:** The cast films of the conjugates were electroactive. We present the electrical characteristics of **8b** and **8c**, for which cast films of suitable and comparable thickness under controlled conditions could be obtained. For comparison, the data relative to the precursor quaterthiophene **3a** (t4-OTHP; see the Supporting Information for the molecular structure) are also given. Cast films of **8b**, **8c**, and the precursor quaterthiophene were deposited onto substrates consisting of two interdigitated Au electrodes fabricated by evaporating gold onto oxidized silicon wafers and patterned with photolithography (see the Experimental Section and Supporting Information). The electrical characterizations were performed at ambient temperature in a home-made chamber both in air and under dynamic vacuum. The procedure was repeated twice with samples from different preparations to ensure reproducibility of the results. When the electrical characterization was performed in air, a dramatic dependence of the current on the environment was observed for conjugates **8b** and **8c** (but not for **3a**). As an example, Figure 4a shows the current density/time ( $J-t$ )

pumping (curve 3). In this case, much lower currents were measured, but the  $J-t$  curve still showed decreasing behavior with time. These findings suggest a space-charge polarization effect of the sample, as a result of ionic currents, likely promoted by moisture and leading to increasing resistivity with time.<sup>[13]</sup> To avoid ionic conduction, the samples were left in the measurement chamber for several hours under dynamic vacuum, until a constant current with time was observed under constant DC applied voltage. Figure 4b shows the current density/voltage ( $J-V$ ) curves for **8b**, **8c**, and **3a** measured at ambient temperature under a dynamic vacuum of  $10^{-4}$  mbar. The figure shows that the reference compound t4-OTHP displays the highest currents, those of **8b** and **8c** are smaller by four and three orders of magnitude, respectively. It should be noted that the samples considered herein are only hole-transporting samples because gold acts as a hole-injecting contact, for which the work function (5.2 eV) is energetically matched to the highest occupied molecular-orbital energy levels of the investigated materials<sup>[6a]</sup> and prevents electron injection from the negatively biased electrode. We observed that for all samples the current density has a good quadratic dependence on the voltage in the high-field region, as better shown in Figure 4b.

This behavior is typical of space-charge limited current (SCLC,<sup>[14]</sup> given by  $j = (9/8)\epsilon_0\epsilon_r\mu V^2 L^{-3}$  in the trap-free regime, where  $\epsilon_0$  is the vacuum permittivity,  $\epsilon_r$  is the relative dielectric constant of the material,  $\mu$  is the charge carrier mobility, and  $L$  is the electrode separation). By setting  $\epsilon_r$  to 3, hole mobilities  $\mu_h$  of  $1.7 \times 10^{-4}$ ,  $2.4 \times 10^{-8}$ , and  $2.0 \times 10^{-7} \text{ cm}^2 \text{ V}^{-1} \text{ s}^{-1}$  were estimated for t4-OHP, **8b**, and **8c**, respectively, from the slope of the linear portion of the  $J-V^2$  curves (Figure 4c). These values are reasonable as the estimated hole mobility for t4-OHP is the same order of magnitude as the field-effect-transistor (FET; a three-electrode device) hole mobility measured for cast films of quaterthiophene,<sup>[6b]</sup> while those of **8b** and **8c** are of the same order as the FET hole mobilities recently measured for cast films of oligo(*p*-phenylene vinylene) functionalized with ureido-*s*-triazine groups.<sup>[15]</sup> Of course, a more precise evaluation of the hole mobilities of conjugates **8a** and **8c** must wait for FET measurements to be carried out. However, what is significant in the present context is that a change in the dinucleotide scaffold leads to almost one order of magnitude difference in the measured currents of **8b** and **8c**. Moreover, it is tempting to make a correlation with CD data and ascribe the higher current measured for **8c** to its more ordered molecular organization. A more detailed description of the electrical behavior of conjugates **8b** and **8c**, including impedance spectroscopy measurements at different degrees of humidity, will be reported elsewhere.

**Molecular modeling:** Theoretical calculations helped to shed light on the molecular mechanism of the self-assembly of conjugates **8a-c**. Conformational preferences and the ability to form stable supramolecular aggregates in solution with water were investigated by molecular mechanics and molecular dynamics calculations. The search of minimum-energy

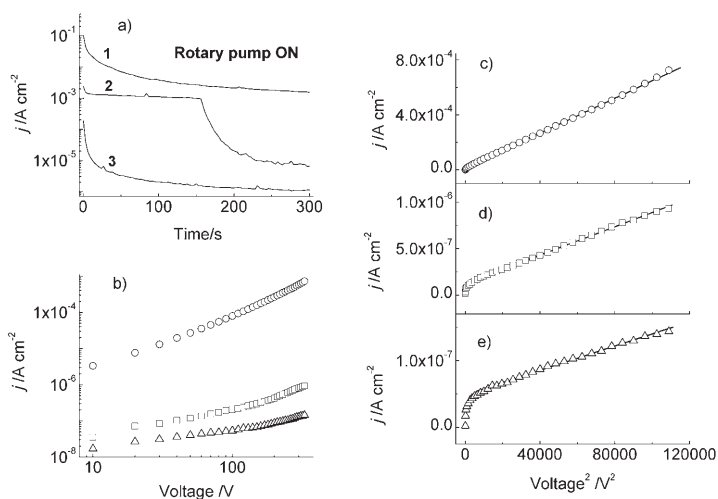


Figure 4. a) Current density versus time for a sample of **8c** at an applied voltage of 100 V: 1) in air, 2) while turning on the rotary pump after 150 s in air, 3) at a pressure of  $10^{-3}$  mbar after 2 h of pumping. b)  $J-V$  characteristics of t4-OTHP (circles), **8c** (squares), and **8b** (triangles) measured at ambient temperature and under a dynamic vacuum of  $10^{-4}$  mbar. Current density versus  $V^2$  for samples of c) t4-OTHP (**3c**), d) **8c**, and e) **8b**. The lines represent the linear fit to the experimental data. The measurements were carried out at ambient temperature and under a dynamic vacuum of  $10^{-4}$  mbar.

curves obtained for **8c** at a constant applied voltage (100 V) under three different conditions. First, the current was measured in air and decreasing values with time at a constant DC voltage were observed (curve 1). Soon after, the current was measured again in air (first portion of curve 2 in Figure 4a) and lower values were obtained, thus indicating that the behavior of the sample is affected by its past treatment. Then the rotary pump was turned on and an abrupt fall in the current was observed (curve 2). Finally, the current was measured at a pressure of  $10^{-3}$  mbar after two hours of

conformations for monomers and dimers was carried out by using simulated annealing protocols in the gas phase and in the presence of the solvent.<sup>[16a]</sup> The calculations were performed within the AMBER force field.<sup>[16b]</sup> Furthermore, an implicit solvent model was used to simulate the presence of water and decreased charges on the phosphate groups to account for the presence of the counterions.<sup>[16c]</sup>

For the monomeric conjugates, two main conformations were found, with *syn* and *anti* oligonucleotide arms with respect to the mean plane of nearly planar t4 (Figure 6). For all systems, the *syn* form was energetically favored over the *anti* form (i.e., by a few kJ mol<sup>-1</sup>; Figure 5). In the *syn* conformation, the dinucleotide arms were folded over the t4 backbone, were aligned at stacking distance, and formed intramolecularly hydrogen-bonded pairs of A...A or T...T. The distance between the  $\pi$  system of t4 and the adjacent base pair falls in the range of 3.3–3.5 Å, as in the  $\beta$  form of DNA<sup>[17]</sup> and close to that found in stilbene–oligonucleotide conjugates,<sup>[18]</sup> but shorter than the distance calculated for the stacks of chiral oligothiophenes (3.7 Å).<sup>[8b]</sup>

The most favored *syn* conformations and stacking distances of the conjugates are reported in Figure 6, which shows that the preferred conformation is made of a hydrophobic core surrounded by phosphate groups. The calculated energy differences between the *syn* and *anti* forms and the base pairs formed in the favored *syn* conformations are shown in the Supporting Information, together with a sketch of the orientation of the ethylene linkers in the different conformations.

During the aggregation process, the *syn* and *anti* monomeric conformations give rise to different supramolecular systems. The free energies of both types of aggregates were calculated using the equation  $\Delta G_{298} = E(\text{MM}) - RT \ln Q$ , where  $E(\text{MM})$  is the energy derived from the molecular modeling and  $Q$  is the partition function. For all the conjugates, the aggregate of the *syn* form is more stable than the aggregate of the *anti* form. The largest difference of  $\Delta G_{298} = -50.16$  kJ mol<sup>-1</sup> is for the **8c** conjugate, and the smallest difference of  $\Delta G_{298} = -20.9$  kJ mol<sup>-1</sup> is for the **8a** conjugate, probably as a result of a greater stabilization of the aggregate of the *anti* form since base pairing occurs between self-complementary bases. The calculated free energies and a sketch of the dimers formed by the *syn* and *anti* conformers

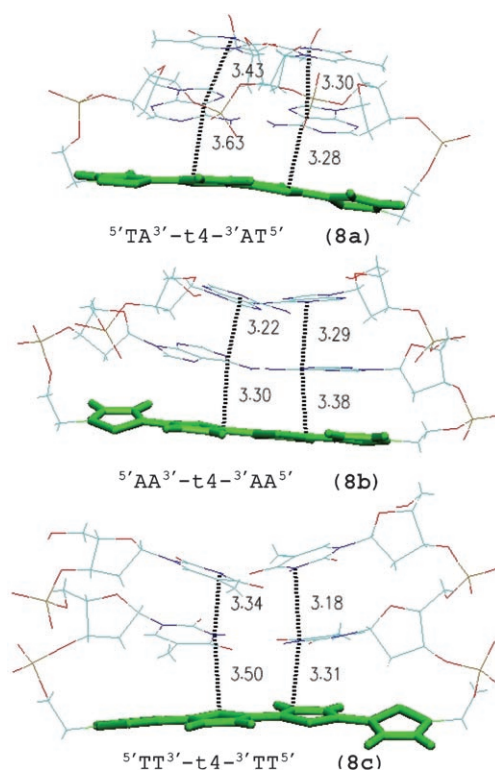


Figure 6. Most favored *syn* conformations and stacking distances of conjugates **8a–c**.

of conjugates **8a–c** are reported in the Supporting Information, together with the electrostatic, van der Waals, and solvation contributions to the total energy. The calculated free energies indicate that the aggregation process is not driven by differences in entropy, as the entropic contribution is very similar for both aggregates.

Figure 7 displays the geometry of the dimers of the favored *syn* forms of **8a–c**, together with the corresponding top views that show the relative orientation of the two t4 moieties. The corresponding dimers of the *anti* form and the orientation of the base pairs in these dimers are shown in the Supporting Information.

The calculations show that the formation of the dimers of the favored *syn* form is driven by the stacking interactions between the upper base pairs at 5' of the first monomer and the quaterthiophene unit of the second monomer to maximize the intermolecular stacking interactions during the aggregation process. Even in **8a** with self-complementary TA ends—because of which there was the possibility that **8a** would form intermolecularly connected A...T Watson and Crick base pairs—the stacking interactions impose the same conformation and aggregation modalities as in the other con-

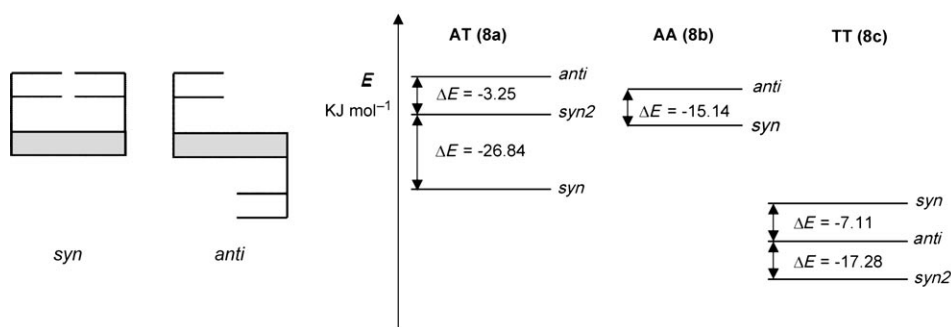


Figure 5. Sketch of the *syn* and *anti* forms of conjugates **8a–c** and the calculated energy differences (kJ mol<sup>-1</sup>). Grey = t4, black = oligonucleotide arms.

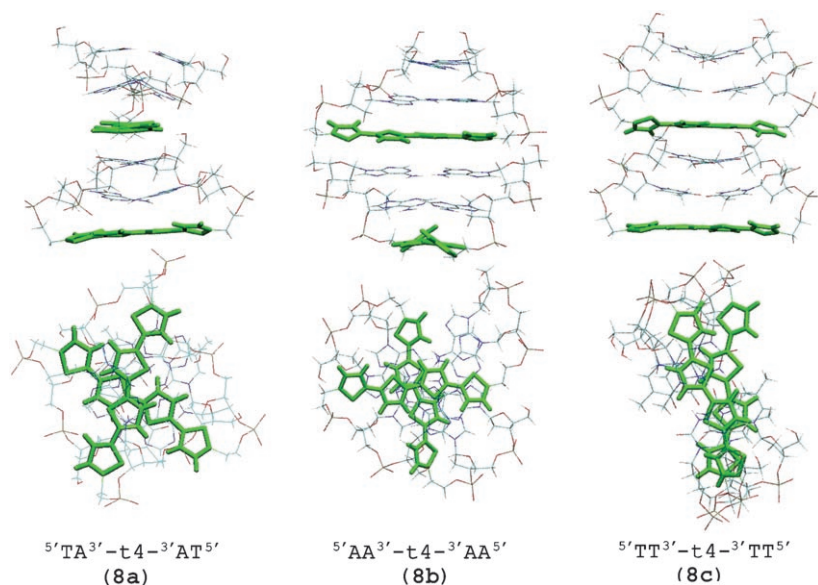


Figure 7. Most stable dimers of conjugates **8a–c** and the corresponding top views showing the relative orientation of the t4 backbones. In **8a** and **8b**, the adjacent t4 units form a nearly perpendicular dihedral angle, while in **8c** they form a dihedral angle of about  $10^\circ$ .

jugates with the formation of intramolecularly connected A...A and T...T base pairs.

The dihedral angle that the quaterthiophene unit of the second monomer forms with the quaterthiophene unit of the first monomer is determined by the orientation of the upper base pair in the single monomer. As a consequence, the t4 moieties within the dimers are rotated with respect to each other by an angle that depends on the nature of the dinucleotide ends. While in the dimers of **8a** and **8b**, the quaterthiophene moieties are almost perpendicular, in the dimer of **8c** they form a dihedral angle of about  $10^\circ$  (Figure 7).

Finally, our calculations (not reported) show that on increasing the number of aggregated molecules the energy difference between the aggregates of the *syn* and *anti* forms increases, with the former becoming more and more favored as a result of the electrostatic contributions to the total energy.

The calculations offer a key to the interpretation of the CD spectra. Besides the intrinsic molecular chirality as a result of the presence of the chiral nucleotide scaffolds, there is an additional supramolecular chirality that arises from the way the molecules pile up during the aggregation process, as indicated by the presence of a CD signal in the region that pertains to the  $\pi$ – $\pi$  transition of t4. Assuming, as is reasonable, that the quaterthiophene transition dipoles are polarized along the long molecular axis, the presence of an exciton coupling in **8c** in solution at high ionic strength (with a  $-/+$  pattern indicative of a right-handed helical organization) is in agreement with the value of  $10^\circ$  calculated for the dihedral angle between adjacent t4 units.<sup>[9,18]</sup> A columnar helical aggregate is formed in which adjacent t4 moieties are progressively staggered by  $10^\circ$  in the same direction; the aggregate is stable enough to be frozen as such in cast film. No exciton coupling is expected when the transi-

tion dipoles are perpendicular,<sup>[9,18]</sup> as indicated by the calculations for **8a,b**. In agreement with this expectation, no exciton coupling is displayed by the CD spectra of these compounds in solution.

The calculations also offer a clue to the understanding of the formation of rod-shaped supramolecular structures in cast films of **8a–c** prepared under quasiequilibrium conditions. The shape and dimension of the aggregates suggest that they are formed through a self-assembly process that starts with *syn*-**8a–c** moieties that pile up in columns. Then side-to-side aggregation of the columns takes place through electrostatic interactions between negatively charged phosphate groups and positively charged counterions that lead to the formation of 2D and 3D rods.

## Conclusion

In conclusion, we have demonstrated that the quaterthiophene–dinucleotide hybrid systems described herein lead to the formation of chiral supramolecular assemblies and afford cast films that are photoluminescent and electroactive. Thiophene–nucleobase stacking interactions orient the molecular conformation towards the form with *syn* dinucleotide ends and the self-assembly modalities towards the formation of columnar aggregates. The films show fine changes in optical and electrical properties on changing the dinucleotide scaffold. These results pave the way to the synthesis of oligothiophene–oligonucleotide hybrid structures in which different competing intra- and intermolecular interactions (thiophene–nucleobase stacking interactions, hydrogen-bonding interactions between nucleobases, oligothiophene–oligothiophene van der Waals interactions, and so forth) can be exploited by varying the oligonucleotide length, substitution pattern, and oligothiophene size to build supramolecular assemblies with programmed functional properties.

## Experimental Section

**Synthesis:** 2-(2-Thienyl)ethanol, 3,4-dihydro-2H-pyran, *para*-toluenesulfonic acid, 2,2 diiodobithiophene (**2**), 2-isopropoxy-4,4,5,5-tetramethyl-1,3,2-dioxaborolane, *n*-butyllithium (2.5 M in hexane), and [1,1'-bis(diphenylphosphino)ferrocene]dichloropalladium are commercially available. The synthesis of compounds **4a–c**<sup>[19]</sup> and **5**<sup>[20]</sup> has been reported elsewhere. The synthesis of compounds **1**, **3a**, **3**, **6a–c**, and **7a–c** is reported in the Supporting Information.

**General procedure for the synthesis of  $\alpha,\omega$ -bis(dinucleotide)-quaterthiophenes 8a–c:** Compounds **7a**, **7b**, or **7c** were dissolved in dry pyridine (3 mL) and treated with  $N^1,N^1,N^3,N^3$ -tetramethylguanidine (0.6 mL) and *syn*-pyridine-2-carboxaldoxime (730 mg) for 16 h at room temperature. The reaction mixture was then added to 30% aqueous ammonia (10 mL) and kept in a sealed flask at 50°C for 24 h. The crude products thus obtained were purified by reversed-phase chromatography on a column of C-18 eluting with a linear gradient of triethylammonium acetate (TEAA) 0.1 M in H<sub>2</sub>O from 0 to 80% of CH<sub>3</sub>CN (300 mL). Compounds **8a–c** were isolated as brown solids after lyophilization in 65–70% yield. **8a**: ESI-MS: calcd for 1652.2; found 1651.7; **8b**: ESI-MS: calcd for 1670.0; found: 669.3. **8c**: ESI-MS: calcd for 1634.0; found: 1633.4.

**UV/Vis spectroscopy:** Absorption spectra were recorded with a Perkin-Elmer Lambda 20 spectrometer in aqueous solution ( $5 \cdot 10^{-6}$  M, pH 7.4) and in cast film on quartz (100  $\mu$ L,  $10^{-3}$  M solution) after solvent evaporation.

**CD spectroscopy:** Spectra were recorded with a spectropolarimeter JASCO J-715 under ambient conditions in aqueous solution ( $\approx 10^{-5}$  M, pH 7.4) and in cast film on quartz (100  $\mu$ L,  $10^{-3}$  M solution) after solvent evaporation.

**Fluorescence microscopy:** Nikon Eclipse 80i optical microscope was used for the optical measurements. The images were recorded with a digital color camera Nikon Digital Sight DS-2mv. The glass substrates were furnished by Knittel gläser and were previously washed with spectroscopic-grade acetone (Aldrich). The films were cast from H<sub>2</sub>O ( $\approx 50$   $\mu$ L,  $10^{-4}$  M) on glass substrates and the solvent was evaporated under a saturated atmosphere.

**Molecular modeling:** The structures of the supramolecular assemblies were fully optimized using the AMBER\* force field. All the molecular mechanics calculations were performed with the MacroModel software package.<sup>[21]</sup>

**Electrical characterization:** Substrates consisted of two interdigitated comb-like gold electrodes (13 pairs of electrode fingers, see the Supporting Information) deposited onto a layer of silicon dioxide thermally grown on silicon plates. The thickness of the oxide was 1  $\mu$ m and the metal layer was 0.6  $\mu$ m. The gaps between the interdigitated electrodes and the width of the Au electrodes were 20 and 40  $\mu$ m, respectively. The length of the Au fingers was 3.0 mm. The surface configuration was chosen to avoid metal diffusion through the organic layer, a common problem of evaporated electrodes onto sandwich-type structures. The organic films were deposited onto the substrates by casting a solution in CHCl<sub>3</sub> (5  $\mu$ L) for t4-OTHP or a solution in water (5  $\mu$ L) for **8b** and **8c** to completely cover the interdigitated area. The concentration of the solutions was 25 g L<sup>-1</sup>, thus leading to films with thicknesses of 0.7–1.0  $\mu$ m greater than that of the electrodes layer, as measured by a Tencor Alpha-step 200 profilometer. The samples were dried under ambient conditions. The electrical characterization was performed at ambient temperature in a home-made chamber both in air and under dynamic vacuum. The characterization in the dynamic vacuum was carried out after several hours of pumping. The current–voltage and current–time measurements were carried out by using a Keithley 487 source-picoammeter.

## Acknowledgements

This study was partially funded by the FIRB RBNE03S7XZ 005 (SYNERGY) project. We thank Prof. Paolo Biscarini (University of Bologna) for helpful discussions and Prof. Duncan Macquarrie (University of York) for the gift of a sample of amylose. We are grateful to Dr. Massimiliano Cavallini (CNR-INSM-Section Bo) for the AFM image reported in the Supporting Information.

- [1] a) A. R. Murphy, J. M. Fréchet, *Chem. Rev.* **2007**, *107*, 1066–1096; b) M. H. Yoon, A. Facchetti, C. E. Stern, T. J. Marks, *J. Am. Chem. Soc.* **2006**, *128*, 5792–5801; c) H. Sirringhaus, *Adv. Mater.* **2005**, *17*,

- 2411; d) G. Barbarella, M. Melucci, G. Sotgiu, *Adv. Mater.* **2005**, *17*, 1581–1593.
- [2] a) H. A. Ho, M. Béra-Abérem, M. Leclerc, *Chem. Eur. J.* **2005**, *11*, 1718–1724; b) A. Herland, P. Björk, K. P. R. Nilsson, J. D. Olsson, P. Åsberg, P. Konradsson, P. Hammarström, O. Inganäs, *Adv. Mater.* **2005**, *17*, 1466–1471; c) H. A. Ho, K. Doré, M. Boissinot, M. G. Bergeron, R. M. Tanguay, D. Boudreau, M. Leclerc, *J. Am. Chem. Soc.* **2005**, *127*, 12673–12676; d) K. Peter, R. Nilsson, O. Inganäs, *Nat. Mater.* **2003**, *2*, 419–424.
- [3] a) B. Liu, G. C. Bazan, *Chem. Mater.* **2004**, *16*, 4467–4476; b) H. A. Ho, M. Boissinot, M. G. Bergeron, G. Corbeil, K. Doré, D. Boudreau, M. Leclerc, *Angew. Chem.* **2002**, *114*, 1618–1621; *Angew. Chem. Int. Ed.* **2002**, *41*, 1548–1551; ; *Angew. Chem. Int. Ed.* **2002**, *41*, 1548–1551, .
- [4] a) F. E. Alemдарoglu, A. Herrmann, *Org. Biomol. Chem.*, **2007**, *5*, 1311–1320; b) K. Tanaka, M. Shionoya, *Chem. Prod. Chem. Letters* **2006**, *35*, 694–699; c) F. D. Lewis, H. Zhu, P. Daublain, T. Fiebig, M. Raytchev, Q. Wang, V. Shafirovich, *J. Am. Chem. Soc.* **2006**, *128*, 791–800; d) K. V. Gothelf, T. H. LaBean, *Org. Biomol. Chem.* **2005**, *3*, 4023–4037; e) F. J. M. Hoeben, E. W. Meijer, A. P. H. J. Schenning, *Chem. Rev.* **2005**, *105*, 1491–1546; f) E. Katz, I. Willner, *Angew. Chem.* **2004**, *116*, 6166–6235; *Angew. Chem. Int. Ed.* **2004**, *43*, 6042–6108; ; g) M. A. Abdalla, J. Bayer, J. O. Radler, K. Müllen, *Angew. Chem.* **2004**, *116*, 4057–4060; *Angew. Chem. Int. Ed.* **2004**, *43*, 3967–3970, .
- [5] a) Y. Tang, F. He, M. Yu, F. Feng, L. An, H. Sun, S. Wang, Y. Li, D. Zhu, *Macromol. Rapid Commun.* **2006**, *27*, 389–392; b) A. Ono, *Macromol. Chem. Phys.* **2006**, *207*, 1629–1632; c) P. Bäuerle, A. Emge, *Adv. Mater.* **1998**, *10*, 324–330.
- [6] a) C. D. Dimitrakopoulos, P. R. L. Malenfant, *Adv. Mater.* **2002**, *14*, 99–117; b) H. E. Katz, J. G. Laquindanum, A. Lovinger, *J. Chemother. J. Chem. Mater.* **1998**, *10*, 633–638; c) R. S. Becker, J. Seixas de Melo, A. L. Maçanita, F. Elisei F. *J. Phys. Chem.* **1996**, *100*, 18683–18695; d) D. Grebner, M. Helbig, S. Rentsch, *J. Phys. Chem.* **1995**, *99*, 16991–16998.
- [7] a) Y. Kanemitsu, K. Suzuki, Y. Masumoto, *Phys. Rev. B* **1994**, *50*, 2301–2305; b) R. S. Becker, J. Seixas de Melo, A. L. Maçanita, F. Elisei, *J. Phys. Chem.* **1996**, *100*, 18683–18695; c) M. Melucci, G. Barbarella, M. Zambianchi, P. Di Pietro, A. Bongini, *J. Org. Chem.* **2004**, *69*, 4821–4828; d) M. Melucci, G. Barbarella, G. Sotgiu, *J. Org. Chem.* **2002**, *67*, 8877–8884.
- [8] a) D. G. Whitten, *Acc. Chem. Res.* **1993**, *26*, 502–509; b) O. Henze, W. J. Feast, F. Gardebien, P. Jonkheijm, R. Lazzaroni, P. Leclère, E. W. Meijer, A. P. H. J. Schenning, *J. Am. Chem. Soc.* **2006**, *128*, 5923–5929; c) F. Meinardi, M. Cerminara, S. Blumstengel, A. Sassella, A. Borghesi, R. Tubino, *Phys. Rev. B* **2003**, *67*, 184205–1–6; d) M. Melucci, G. Barbarella, M. Gazzano, M. Cavallini, F. Biscarini, A. Bongini, F. Piccinelli, M. Monari, M. Bandini, A. Umani-Ronchi, P. Biscarini, *Chem. Eur. J.* **2006**, *12*, 7304–7312.
- [9] a) *Circular Dicroism*, (Eds.: N. Berova, K. Nakanishi, R. W. Woody), Wiley, New York, **2000**; b) *Circular Dichroic Spectroscopy*, (Eds.: N. Harada, K. Nakanishi), Oxford University Press, Oxford, **1983**.
- [10] F. D. Lewis, L. Zhang, X. Liu, X. Zuo, D. M. Tiede, H. Long, G. C. Schaz, *J. Am. Chem. Soc.* **2005**, *127*, 14445–14453.
- [11] H. W. Jun, S. E. Paramonov, J. D. Hartgerin, *Soft Matter* **2006**, *2*, 177–181.
- [12] K. Ohdan, K. Fujii, M. Yanase, T. Takaha, T. Kuriki, *Biocatal. Bio-transform.* **2006**, *24*, 77–81.
- [13] D. R. Lamb, *Electrical Conduction Mechanisms in Thin Insulating Films*, Methuen, London, **1967**.
- [14] M. A. Lampert, P. Mark, *Current Injection in Solids*, Academic Press, New York, **1970**.
- [15] P. Jonkheijm, N. Stutzmann, Z. Chen, D. M. de Leeuw, E. W. Meijer, A. P. H. J. Schenning, A. P. H. J. , F. Würthner, *J. Am. Chem. Soc.* **2006**, *128*, 9535–9540.
- [16] a) A. Acocella, A. Venturini, F. Zerbetto, *J. Am. Chem. Soc.* **2004**, *126*, 2362–2367; b) J. Scott, P. A. Weiner, D. A.; Kollman, U. Case, *J. Comput. Chem.* **1990**, *11*, 440–467; c) C. Singh, C. Ghio, G. Alago-

- na, S. Profeta, P. Weiner, *J. Am. Chem. Soc.* **1984**, *106*, 765–784;  
d) W. Clark Still, A. Tempczyk, R. C. Hawley, T. Hendrickson, *J. Am. Chem. Soc.* **1990**, *112*, 6127–6129.
- [17] *Nucleic Acids. Structures, Properties and Functions* (Eds.: V. A. Bloomfield, D. Crothers, I. Tinoco), University Science Books, Sausalito, CA, **2000**.
- [18] F. D. Lewis, L. Zhang, X. Liu, X. Zuo, D. M. Tiede, H. Long, G. C. Schaz, *J. Am. Chem. Soc.* **2005**, *127*, 14445–14453.
- [19] M. Cirilli, F. Bachechi, G. Ughetto, F. P. Colonna, M. L. Capobianco, *J. Mol. Biol.* **1993**, *230*, 878–889.
- [20] J. E. Marugg, M. Tromp, P. Jhuran, C. F. Hoyng, G. A. van der Marel, J. H. van Boom, *Tetrahedron* **1984**, *40*, 73–78.
- [21] F. Mohamadi, N. G. J. Richards, W. C. Guida, R. Liskamp, M. Lipton, C. Caufield, G. Chang, T. Hendrickson, W. C. Still, *J. Comput. Chem.* **1990**, *11*, 440–467.

Received: June 21, 2007

Revised: August 29, 2007

Published online: October 12, 2007